energies

MDPI

Article

Implementation and Adaptability Analysis of Numerical Simulation for Shale Oil CO_2 Huff and Puff

Fenglan Zhao [1], Yu Wang [1,2], Shijun Huang [1,*], Miaomiao Liu [1] and Changhe Yang [1]

[1] College of Petroleum Engineering, China University of Petroleum (Beijing), Beijing 102249, China; zhfl@cup.edu.cn (F.Z.); wy1012_cq@petrochina.com.cn (Y.W.); 2023310122@student.cup.edu.cn (M.L.); 2022210410@student.cup.edu.cn (C.Y.)
[2] Changqing Oilfield Branch No. 1 Oil Production Plant, Yan'an 716009, China
* Correspondence: hshj@cup.edu.cn

Abstract: Carbon dioxide (CO_2) is being considered for use to enhance oil recovery and resource utilization and storage, with wide technical adaptability. In this paper, a numerical simulation method is used to study the adaptability of CO_2 huff and puff in shale reservoirs. A fluid model introduces the nanoconfinement effect and reflects the nanoconfinement effect using the fluid *p*–*T* phase diagram. This method uses local grid refinement and changes the permeability near the grid to characterize the reservoir reconstruction volume (SRV) fracture network while considering the CO_2 diffusion effect. The results indicate that by using the incremental recovery rate and oil change rate as references, adaptive charts can be obtained for different K_f/K_m and oil saturation. When K_f/K_m is 1000 and the increase in the CO_2 recovery rate reaches 1.5%, the lower limit of oil saturation is 0.54. When K_f/K_m is 1000 and the increase in the CO_2 recovery rate reaches 2%, the lower limit of oil saturation is 0.57. When the oil saturation is 0.5 and the CO_2 huff and puff oil change rate reaches 0.3, the lower limit of K_f/K_m is 700. Finally, when the oil saturation is 0.548 and the CO_2 huff and puff oil change rate reaches 0.6, the lower limit of K_f/K_m is 10. The research results are significant and can guide the design and application of on-site CO_2 throughput test plans.

Keywords: CCUS; shale oil; CO_2 huff and puff; adaptability analysis; enhanced oil recovery

check for updates

Citation: Zhao, F.; Wang, Y.; Huang, S.; Liu, M.; Yang, C. Implementation and Adaptability Analysis of Numerical Simulation for Shale Oil CO_2 Huff and Puff. *Energies* **2024**, *17*, 454. https://doi.org/10.3390/en17020454

Academic Editors: Edo Boek and Mofazzal Hossain

Received: 10 November 2023
Revised: 21 December 2023
Accepted: 9 January 2024
Published: 17 January 2024

Copyright: © 2024 by the authors. Licensee MDPI, Basel, Switzerland. This article is an open access article distributed under the terms and conditions of the Creative Commons Attribution (CC BY) license (https://creativecommons.org/licenses/by/4.0/).

1. Introduction

Under China's vision of "peak carbon emissions by 2030 and carbon neutrality by 2060", the development and application of CCUS technology for carbon capture, utilization, and storage are garnering increasing attention. CO_2 technology has a wide adaptability, a significant oil-increasing effect, and can be recycled, gradually becoming one of the most attractive applications of CCUS technology [1–3]. Shale reservoirs have high geological reserves of crude oil with good properties, but shale reservoirs cannot achieve high recovery rates due to water injection difficulties. Gas injection has technical advantages for this type of reservoir and can effectively improve oil recovery, while CO_2 can significantly improve crude oil fluidity and supplement formation energy. CO_2 huff and puff can increase single-well production in a relatively short period of time. Therefore, the systematic study of shale oil CO_2 huff and puff adaptability is highly significant [4–6].

Hydraulic fracturing is widely used in unconventional oil and gas resource development as a means of effectively increasing the permeability of unconventional reservoirs [7]. In unconventional fractured reservoirs, previous discrete fracture network modeling techniques have been able to characterize natural fracture networks efficiently and establish the corresponding numerical simulation models to predict the propagation patterns of hydraulic fracturing [8]. A variety of theoretical solution models for hydraulic fracturing have been developed [9] due to the limited factors considered in theoretical derivations. These assume that fractures formed by hydraulic fracturing in reservoirs are straight while the rock matrix is isotropic and that corresponding theoretical solutions can be derived

following further assumptions of the cross-sectional characteristics of hydraulic fractures. This significantly facilitates preliminary predictions regarding reservoir hydraulic fracturing, which were made by engineers in early research. However, with the development of monitoring technology, it has been confirmed that hydraulic fractures are characterized by bending and branching in rocks and reservoirs [10], indicating that theoretical models are insufficient in precisely predicting the morphology of reservoir hydraulic fractures. In addition, there are difficulties in the preparation of samples for laboratory experiments and high costs associated with field trials, making it difficult to quantify complex fractures in theoretical derivations. As a result, numerical simulation has become an effective approach for investigating the propagation patterns of hydraulic fractures in heterogeneous reservoirs. One oil field in Jiangsu, China, conducted the first CO_2 huff and puff test on Well Su 88. The cumulative CO_2 injection volume was 116 t, and the recovery rate increased by 5%. This indicates that CO_2 huff and puff has a good adaptability for fault block reservoirs with a small reservoir area, low reserves, and poor interlayer continuity. Jin et al. conducted carbon dioxide huff and puff experiments using core samples, and the results showed that supercritical CO_2 can extract hydrocarbons such as methane, ethane, and propane from the core. Based on the experimental results, the feasibility of CO_2 huff and puff in improving oil recovery and CO_2 storage in Bakken shale oil reservoirs was proposed [11]. Francisco D Tovar et al. conducted the first comprehensive experimental evaluation of organic rich shale, as well as 18 core CO_2 huff and puff experiments to evaluate the effects of the shut-in time, injection pressure, and minimum miscibility pressure on oil recovery, demonstrating the potential for CO_2 to replace crude oil in organic shale reservoirs [12]. Gamadi T.D. et al. conducted simulation research on gas injection huff and puff based on the established single-well model for the multi-stage fracturing of horizontal wells. The results showed that the recovery rate improved after gas injection and stimulation but that the recovery rate of highly heterogeneous formations was higher than that of homogeneous formations. This is because, for homogeneous formations, injected CO_2 is prone to diffusion into the interior of the reservoir, resulting in poor pressure suppression during the closed-well stage and lower oil recovery [13]. Chen et al. established a component model to simulate the CO_2 throughput process. Research has shown that compared to depleted mining, the recovery rate after CO_2 huff and puff decreases and that the longer the gas injection time, the greater the reduction in the recovery rate. Therefore, it can be concluded that in depleted mining or CO_2 huff and puff, the stronger the heterogeneity of shale oil reservoirs, the lower the recovery rate [14]. Orozco et al. conducted historical fitting on the field data of gas injection huff and puff experiments in the Eagle Ford block, and, based on this, conducted CO_2 huff and puff prediction. The results indicated that CO_2 throughput can significantly improve the recovery efficiency of the Eagle Ford block [15]. In summary, worldwide, there is relatively little research on the mathematical modeling of CO_2 throughput related to the comprehensive consideration of the nanoconfinement effect and the complex fracture network in shale oil, and there is no corresponding evaluation of the advantages and disadvantages of shale oil reservoirs. In addition, the adaptability limit of oil reservoirs has not been determined. Therefore, it is necessary to conduct a systematic analysis of the adaptability of shale oil CO_2 huff and puff.

The Chang 7 reservoir in the Ordos Basin is a typical shale oil reservoir with poor reservoir properties and developed natural fractures. Therefore, in response to the current problems of energy depletion and low recovery after depleted development, an evaluation of the adaptability of shale oil CO_2 huff and puff was carried out, and the ratio of the permeability to matrix permeability (K_f/K_m) and the adaptability range of oil saturation CO_2 huff and puff in the SRV transformation area were studied, providing a theoretical reference for shale oil development.

2. Establishment of a Numerical Model for Shale Oil Fracturing Horizontal Wells

The natural fractures in the Ordos Basin were developed and connected to each other. Artificial fractures control the oil drainage area, making them a storage space

and seepage channel for shale reservoirs [16,17]. A dual medium model was established based on geological data of the Chang 7 shale reservoir, with a component model size of 76 × 21 × 4, each grid in the *i*-direction being 20 m, each grid in the *j*-direction being 20 m, and a layer thickness of 12 m. The top buried depth was 2100 m, the reference pressure was 18.1 MPa, the porosity was 10%, the matrix permeability was 0.02×10^{-3} μm^2, the reservoir temperature was 71.71 °C, and the initial oil saturation was 0.6. There was a single horizontal well in the middle of the model, with a perforated interval in the third layer and a horizontal interval length of 1200 m. The established CO_2 huff and puff numerical model for shale oil horizontal wells is shown in Figure 1.

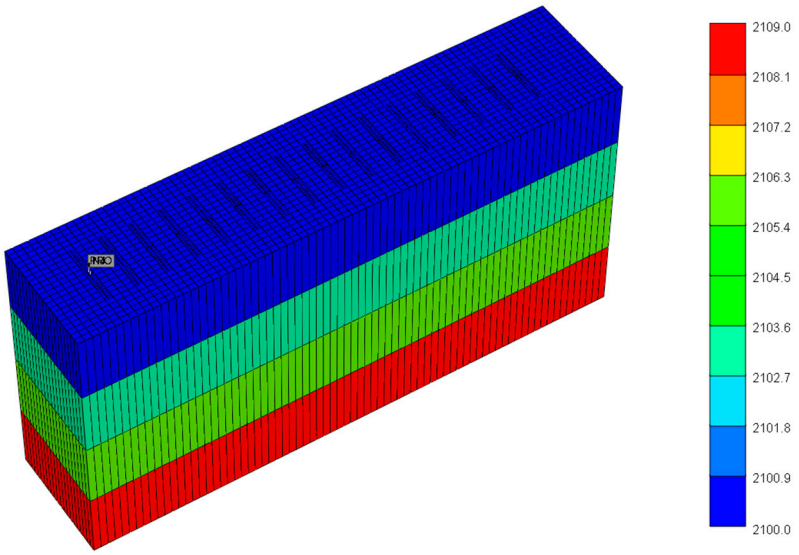
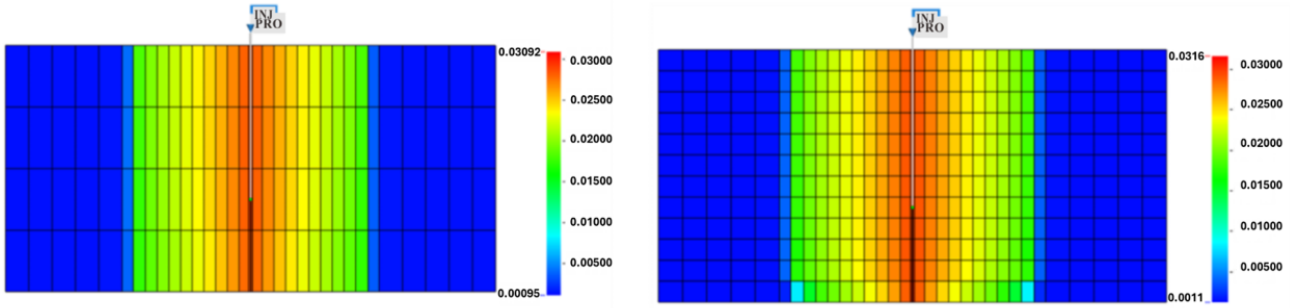


Figure 1. CO_2 huff and puff model of shale oil.

Before conducting numerical simulation experiments, a model with 4 and 12 vertical layers was established for comparison, while the other parameters remained unchanged. The CO_2 mole fraction field in the oil phase after well closure is shown in Figure 2. Figure 2a shows 4 vertical layers, while Figure 2b shows 12 vertical layers.

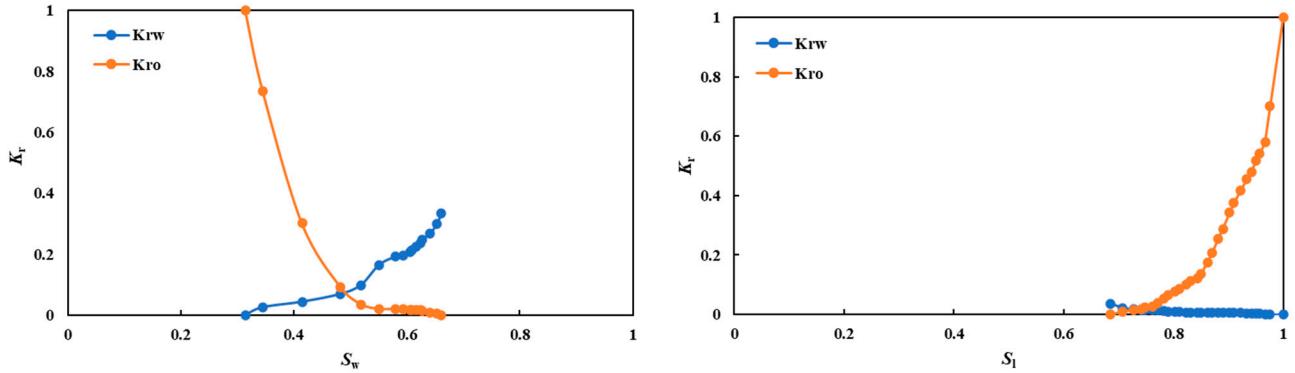


(**a**) (**b**)

Figure 2. CO_2 mole fraction in oil phase aftersoaking: (**a**) 4 layers; and (**b**) 12 layers.

As seen in Figure 2, there is little difference in the CO_2 mole fraction field in the oil phase after the model is divided into 4 and 12 vertical layers. Considering the calculation speed and performance characterization of the model, this study was conducted on the model with four vertical layers.

Oil water and oil gas relative permeability curves are shown in Figure 3.



(**a**) (**b**)

Figure 3. Relative permeability curve: (**a**) oil water relative permeability curve; and (**b**) oil gas relative permeability curve.

The basic parameter values of the model are shown in Table 1, which were determined based on the physical properties of the Chang 7 shale oil reservoir, and the relative permeability curves are shown in Figure 3.

Table 1. Basic parameter values of the model.

Parameter	Basic Value
Matrix permeability/10^{-3} μm^2	0.02
Oil saturation	0.6
K_f/K_m	10
Horizontal well section length/m	1200
Reservoir thickness/m	12
Soaking time/d	30
Artificial crack half-length/m	100

3. A Fluid Model Considering the Nanoconfinement Effect

Nanoscale pore throat systems are commonly developed in shale oil reservoirs, and the main reservoir space is composed of pores with pore sizes of 50–300 nm, with locally developed micron-sized pores. Research in the field of shale oil reservoir development has shown that the presence of nanoscale pores and throats in shale reservoirs can lead to significant capillary pressure. Capillary pressure affects the thermodynamic phase behavior of crude oil components, and phase behavior affects the calculation of components and fluid flow in porous media, thereby affecting crude oil production [18–21]. Therefore, application of the nanoconfinement effect is of great significance in shale oil reservoir development.

According to the literature, it is known that critical pressure and temperature changes can be used to simulate the influence of nanoconfinement effects on phase behavior [22]. The research results indicate that the shift in critical properties of nanoconfined fluids is related to the ratio of the Lennard-Jones size parameters to the pore radius (dimensionless pore radius, σ_{LJ}/r_p). The relationship between critical pressure and critical temperature is shown in Equations (1)–(3) [23–25].

$$\Delta T_c^* = \frac{T_{cb} - T_{cp}}{T_{cb}} = 0.9409\frac{\sigma_{LJ}}{r_p} - 0.2415\left(\frac{\sigma_{LJ}}{r_p}\right)^2 \quad (1)$$

$$\Delta p_c^* = \frac{p_{cb} - p_{cp}}{p_{cb}} = 0.9409\frac{\sigma_{LJ}}{r_p} - 0.2415\left(\frac{\sigma_{LJ}}{r_p}\right)^2 \quad (2)$$

$$\sigma_{LJ} = 0.244\sqrt[3]{\frac{T_{cb}}{p_{cb}}} \quad (3)$$

In the equation, ΔT_c^* is the change in relative critical temperature caused by the nanoconfinement effect, K; Δp_c^* is the change in relative critical pressure caused by the nanoconfinement effect, atm; T_{cb} is the critical temperature of the component, K; T_{cp} is the component-corrected critical temperature, K; p_{cb} is the critical pressure of the component, atm; p_{cp} is the component corrected critical pressure, atm; r_p is the aperture radius, nm; and σ_{LJ} is the Lennard-Jones size parameter, nm.

Due to the significant impact of the number of fluid model components on the accuracy and speed of numerical simulation calculations, it is necessary to balance calculation accuracy and time. To avoid affecting the simulation results, multiple components of crude oil were merged into seven pseudo-components based on the principle of similar composition properties, as shown in Table 2.

Table 2. Classification of crude oil components.

Original Component	Mole Fraction/%	Pseudo-Component	Mole Fraction/%
CO_2	0.11	CO_2	0.11
N_2	1.37	N_2~CH_4	28.69
CH_4	27.32		
C_2H_6	8.66	C_2H_6~nC_6	32.10
C_3H_8	10.05		
iC_4	1.64		
nC_4	4.45		
iC_5	1.56		
nC_5	2.22		
nC_6	3.52		
nC_7	4.62	nC_7~nC_{10}	14.76
nC_8	3.93		
nC_9	3.41		
nC_{10}	2.80		
C_{11}-C_{14}	8.91	C_{11}~C_{21}	17.39
C_{15}-C_{18}	5.65		
C_{19}-C_{21}	2.83		
C_{22}-C_{25}	2.54	C_{22}~C_{30}	4.46
C_{26}-C_{30}	1.91		
C_{31+}	2.49	C_{31+}	2.49

The relative volume fitting of the constant component expansion experiment (CCE) is shown in Figure 4. It can be seen that the fitting degree of the pseudo-component crude oil phase is relatively high, so this model can be used for subsequent numerical simulation research. The pore throat structure of block Chang 7 varies greatly, with pore radii ranging from 2 to 8 μm. The throat radius range is 20 to 150 nm [26]. In the process of fluid migration, the nano throat has a significant impact on the phase behavior of fluid components. The critical parameters of pseudo-components in crude oil are shown in Table 3.

Since the pore throat structure of the actual block is complex, the arithmetic mean standard value of the throat is 80 nm. The corrected critical parameters are shown in Table 4.

Figure 5 shows the *p*–*T* phase diagram of the original and modified critical parameters. It can be seen that the corrected *p*–*T* phase diagram shifts upwards and the bubble point pressure increases, thereby affecting crude oil simulation development. Therefore, this demonstrates the significance of the nanoconfinement effect in studying CO_2 huff and puff development.

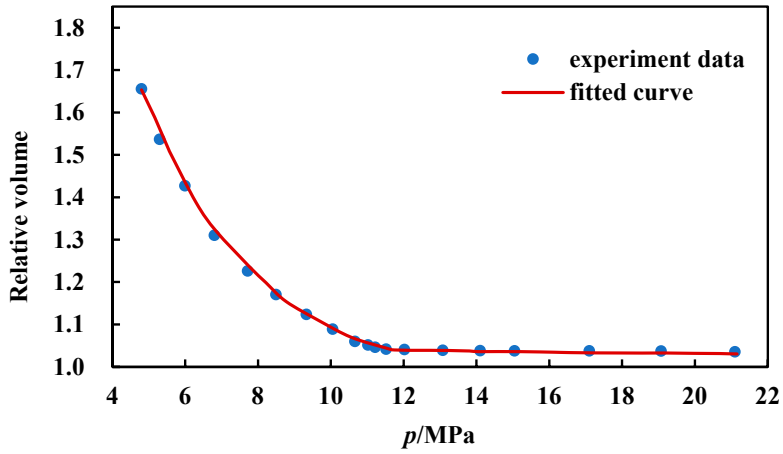


Figure 4. Relative volume fitting in constant component expansion experiment (CCE).

Table 3. Critical parameters of proposed components.

Component	CO_2	N_2~CH_4	C_2H_6~nC_6	nC_7~nC_{10}	C_{11}~C_{21}	C_{22}~C_{30}	C_{31+}
p_{cb}/atm	72.80	44.86	39.90	25.05	15.41	9.33	6.95
T_{cb}/K	304.20	187.38	395.70	576.47	791.97	915.44	1121.75

Table 4. Correction of critical parameters based on average throat radius.

Component	CO_2	N_2~CH_4	C_2H_6~nC_6	nC_7~nC_{10}	C_{11}~C_{21}	C_{22}~C_{30}	C_{31+}
p_{cb}/atm	72.60	44.66	39.67	24.86	15.25	9.21	6.84
T_{cb}/K	302.88	186.57	393.41	572.06	784.07	904.13	1105.41

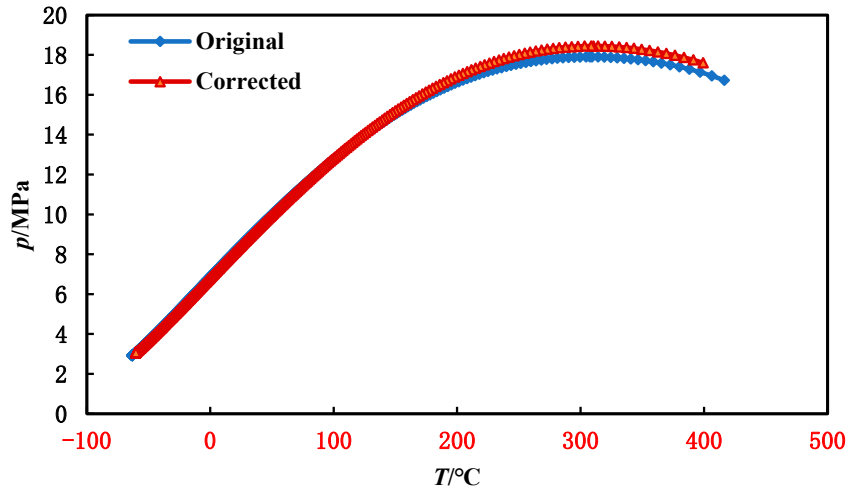


Figure 5. *p*–*T* phase diagram of original critical parameters and modified critical parameters.

4. SRV Regional Fracture Network Model for Shale Oil Horizontal Wells

Hydraulic fracturing simulation is an important component of shale oil development. At present, there are four types of crack models: continuous medium model, equivalent continuous medium model, discrete crack, and embedded discrete crack [27,28]. The continuous medium and equivalent continuous medium models have a wide range of applications and simple processing methods, resulting in high computational efficiency. However, they cannot accurately characterize the complex fracture network formed by natural and artificial fracture systems. The division of discrete crack grids is complex

and can represent complex crack networks, but the computational efficiency is low and deviations are prone to occurring during the calculation process. Embedded discrete cracks reduce computational bias and improve computational efficiency by replacing unstructured grids with regularized grids.

The schematic diagram of the actual SRV fracture network after fracturing is shown in Figure 6, where ① is the main fracture area, ② is the SRV transformation area, and ③ is the pure matrix area.

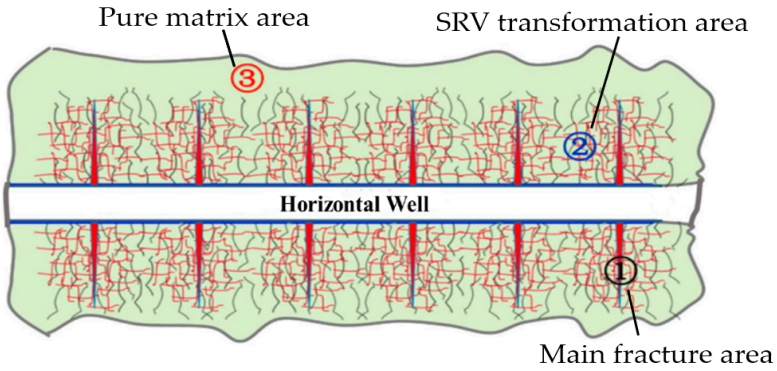


Figure 6. SRV area sewing mesh.

(1) Construction of a matrix and natural fracture system

We established a dual medium model, input the permeability of the matrix system and natural fracture system, and then divided the model into two regions based on the equivalent continuous medium model, namely, the equivalent region composed of the natural fracture system and the matrix region, and the pure matrix region.

(2) Construction of a hydraulic fracturing system

Due to the complex distribution of natural and artificial fractures after volume fracturing, it is easy to form a complex network of fractures; however, this results in an inability of the continuous medium model to accurately depict the fracture morphology after fracturing. Therefore, artificial fractures are created through local grid refinement, i.e., by locally densifying the grid where the artificial crack is located into multiple sub-grids, setting the width of the middle sub-grid to represent the width of the main crack, changing the initial permeability of the sub-grid, and characterizing the conductivity of the main crack through effective permeability. The calculation formula for effective permeability is determined using Equation (4):

$$K_{\mathrm{eff}} = (\mathrm{W_f} \times K_{\mathrm{int}}) \div \mathrm{W_{inner}} + K_{\mathrm{f}} \quad (4)$$

In the equation, K_{eff} refers to the effective permeability, 10^{-3} μm^2; $\mathrm{W_{inner}}$ refers to the calculation of the effective permeability parameter (the crack width set to maintain the original crack conductivity, usually taken as the default value of 0.6096 m), 10^{-3} μm^2; $\mathrm{W_f}$ refers to the width of the main crack, m; K_{int} refers to the initial original permeability, 10^{-3} μm^2; and K_{f} is the set natural fracture permeability, 10^{-3} μm^2.

The effective permeability of artificial fractures was calculated to be 500×10^{-3} μm^2 according to Equation (4).

(3) Simulation of SRV fracture network

To simulate the SRV area around the main fracture more accurately after hydraulic fracturing, the permeability of the grid refinement area, except for the main fracture, was appropriately increased, thereby simulating the high-conductivity area formed after fracturing. The crack network model established using the numerical simulation method is shown in Figure 7, where ① is the main crack area, ② is the SRV modification area, and ③ is the pure matrix area.

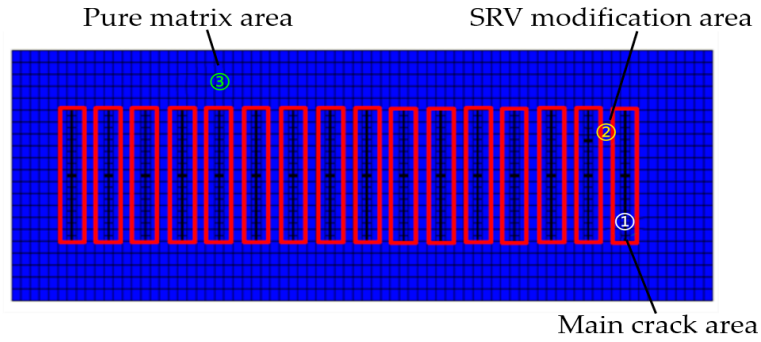


Figure 7. Schematic diagram of SRV mesh numerical simulation characterization.

From the perspective of economy and production development, each production well has a limited production capacity. Once the actual production capacity is less than this limited production capacity, taking into account the production cost and other factors, there is no need to continue mining under this technical plan. Further measures to increase production capacity need to be established during the development process, taking the oil production rate as the standard, comprehensively considering the factors of drilling, completion, and operating costs, and determining the production time. Therefore, in conjunction with the site, the maximum production capacity of the wellhead can be introduced. The economic limit chart of deep CO_2 flooding in different oil layers is shown in Figure 8 [29].

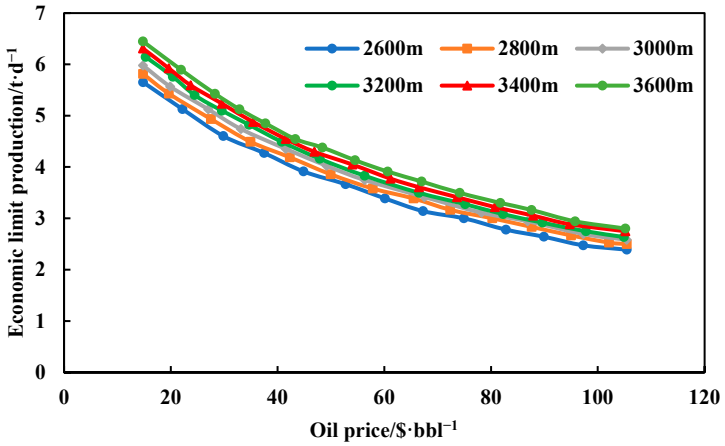


Figure 8. Economic limit chart of CO_2 flooding in different oil layers.

As shown in Figure 8, when the middle depth of the oil layer is 2106 m, based on the current oil price of USD 80 per barrel, the economic limit production of CO_2 flooding in the chart is close to 3 m^3/d. Therefore, based on the chart and the actual development situation of the Chang 7 shale reservoir, the maximum production capacity of the wellhead is set at 3 m^3/d. If the actual production rate is greater than 3 m^3/d, it will normally proceed to the next round of stimulation, and when the daily oil production rate is less than 3 m^3/d, the production well will be closed and the production stopped.

Taking the increase in oil production (the difference between the cumulative oil production of throughput development and the cumulative oil production of depletion development) as a reference indicator, the influence of the SRV region's fracture network on the throughput development effect is characterized by changing the permeability of the SRV region, thereby demonstrating the applicability of the established fracture network model. The permeability K_f of the SRV renovation area was changed to 2×10^{-3} μm^2 and 20×10^{-3} μm^2, and the throughput development effects were compared under two different permeability sizes, as shown in Figure 9.

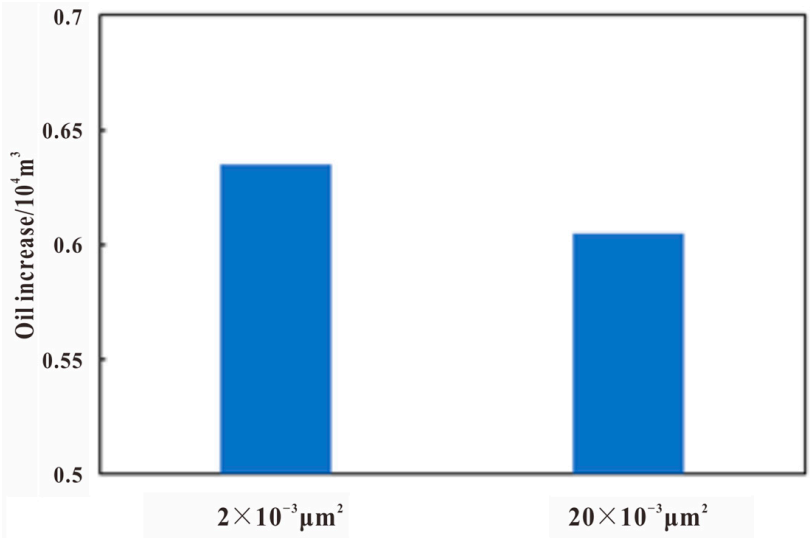


Figure 9. Oil increase under different SRV permeabilities.

It can be seen in Figure 9 that as K_f increases, the oil increase declines and the CO_2 stimulation effect weakens. This is because as K_f increases, CO_2 gas is prone to gas channeling. At the same time, during the development process, gas will be extracted along the seepage channel, resulting in a less significant stimulation effect. Therefore, the established seam mesh model has a good applicability and can be used in subsequent research.

5. Considering the CO_2 Diffusion Effect

The diffusion of gas molecules plays an extremely important role in improving oil recovery during CO_2 throughput. Research has shown that the diffusion coefficient affects the dissolution and diffusion time of CO_2 in oil. During the CO_2 huff and puff process, the injection effect of huff and puff is greatly affected by the CO_2 diffusion coefficient, which in turn affects the final recovery degree of crude oil. Therefore, the influence of CO_2 molecular diffusion should be properly considered in the model to simulate the CO_2 throughput process more effectively and provide a foundation for subsequent research.

The CO_2 diffusion coefficient is a complex function of reservoir temperature, pressure, and fluid properties. In some cases, the estimated values obtained using the above equations have significant deviations from experimental data, and research has shown that the diffusion coefficients of specific reservoirs are generally determined experimentally, while the diffusion coefficients of multi-component oil and gas systems are more difficult to determine in this way [30–32]. The measured values of some crude oil diffusion coefficients are shown in Table 5, based on comprehensive research in the literature [33–35]. In this case, the software can choose to input diffusion coefficients from experimental data or published articles. The reference literature refers to a tight oil reservoir with similar physical parameters, and thus a diffusion coefficient of 500 × 10^{-9} m^2/s can be set.

Table 5. Diffusion coefficient of CO_2 in crude oil under different conditions.

	Pressure/MPa	Temperature/°C	Permeability/10^{-3} μm^2	Diffusion Coefficient/10^{-9} m^2·s^{-1}
Tight oil	6.5~30	70~150	/	0.0246~2.8274
	15~30	20~80	/	0.2~5.45
	20	60	0.08	500

To better reflect the influence of molecular diffusion during the shale oil CO_2 huff and puff process, taking the first round of huff and puff as a reference, the CO_2 molar fraction fields in the oil phase after gas injection and after the end of the closed well were compared, with and without the consideration of molecular diffusion, as shown in Figures 10 and 11.

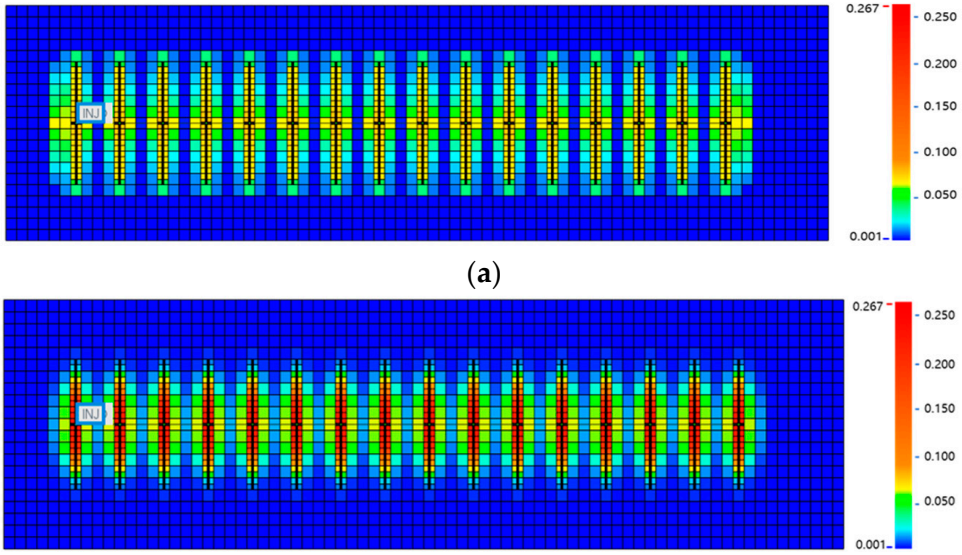


Figure 10. Molar fraction field diagram of CO_2 in the oil phase after injection: (**a**) considering CO_2 diffusion; and (**b**) not considering CO_2 diffusion.

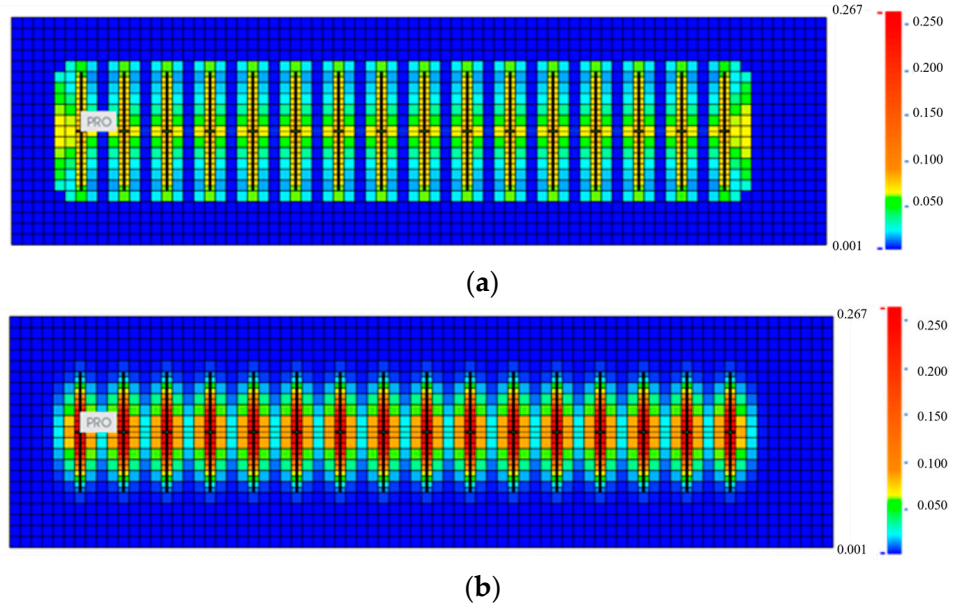


Figure 11. Molar fraction field diagram of CO_2 in the oil phase after soaking time: (**a**) considering CO_2 diffusion; and (**b**) not considering CO_2 diffusion.

Figure 10a represents the variation in the CO_2 mole fraction in the oil phase after a gas injection, considering the effect of CO_2 diffusion, while Figure 10b represents the variation in the CO_2 mole fraction in the oil phase after a gas injection but without considering CO_2 diffusion. After gas injection, the extension of the grid considering CO_2 diffusion is wider than that without diffusion, and the mole fraction of CO_2 in the oil phase, considering diffusion in the corresponding grid, is smaller. This is because at the same gas injection rate, the diffusion-considered CO_2 diffuses more into the matrix. Figure 11 represents the variation in the CO_2 mole fraction in the oil phase with and without CO_2 diffusion consideration after well closure, resulting in a smaller mole fraction of CO_2 in the matrix grid near the fracture zone, compared to when CO_2 diffusion was not considered, and a wider coverage range.

The final recovery degree with and without diffusion consideration is shown in Figure 12. It can be seen from the graph that the recovery rate corresponding to CO_2 diffusion is 24.59%, which is 1.44 percentage points higher than that without CO_2 diffusion. Therefore, the diffusion effect in CO_2 throughput cannot be ignored and is an important mechanism in the simulation process.

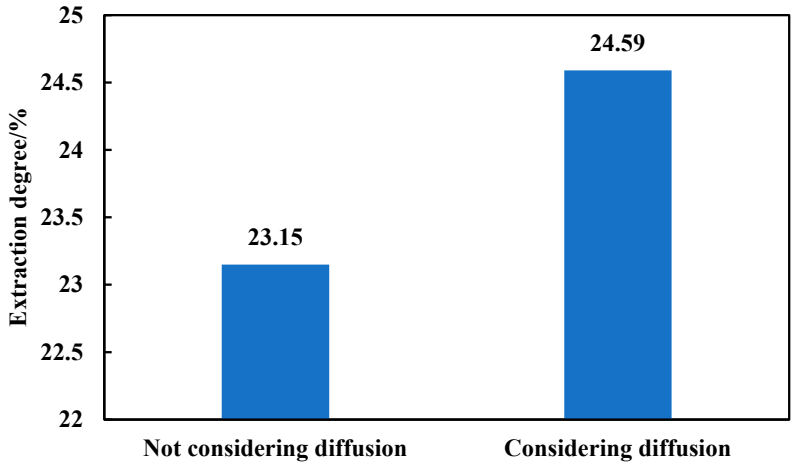


Figure 12. Degree of extraction not considering diffusion and considering diffusion.

6. Adaptability Analysis of Shale Oil CO_2 Huff and Puff

In order to explore the development effect of CO_2 huff and puff under the coupling effect of K_f/K_m and oil saturation, numerical simulation methods were used to study the adaptability limits of CO_2 huff and puff development, with the increase in the recovery degree and oil change rate being reference indicators.

The incremental recovery degree is defined as the difference between the recovery degree of huff and puff development and the recovery degree of depletion development. The oil change rate is the ratio of the increased oil amount to the cumulative CO_2 injection amount during the huff and puff process. The depletion production time is set to be the same as the actual huff and puff production time [36]. The oil change rate is determined using Equations (5)–(7):

$$\Delta Q = Q_1 - Q_2 \tag{5}$$

$$\Delta Q' = \rho_o \Delta Q \tag{6}$$

$$R = \frac{\Delta Q'}{G_g} \tag{7}$$

In the equations, Q_1 represents the cumulative oil production through throughput, 10^4 m^3; Q_2 represents the cumulative oil production due to depletion, 10^4 m^3; $\triangle Q$ represents the oil increase, 10^4 m^3; $\triangle Q'$ represents the oil increase, 10^4 t; ρ_o represents the density of crude oil, taken as 840 kg/m^3; G_g represents the cumulative injection amount of CO_2, 10^4 t; and R represents the oil change rate, t/t.

7. Adaptability Analysis of K_f/K_m

K_f/K_m is an important parameter that affects shale oil reservoir development. In order to study the incremental recovery and oil change rate of CO_2 huff and puff under different K_f/K_m conditions, CO_2 huff and puff simulations were conducted by setting K_f/K_m to 10, 100, and 1000, respectively, when the oil saturation was 0.6. Using the incremental recovery rate and oil change rate as evaluation indicators for development effectiveness, the development effectiveness under different K_f/K_m was compared, and the results are shown in Table 6 and Figure 13.

Table 6. Development effect under different K_f/K_m.

K_f/K_m	Increment of Extraction Degree/%	Oil Exchange Ratio
10	2.2032	0.7919
100	2.1103	0.6302
1000	2.0132	0.5153

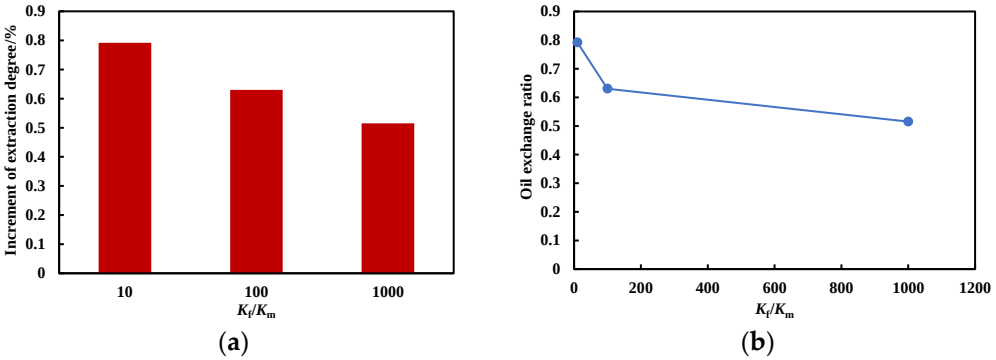


Figure 13. Incremental recovery degree and oil change rate at different K_f/K_m: (**a**) increment in extraction degree; and (**b**) oil exchange ratio.

When the oil saturation is constant, with the increase in K_f/K_m, the incremental recovery degree and oil change rate continue to decrease. The decrease in recovery degree is slow, and the oil change rate first increases and then decreases slightly. When K_f/K_m is 10, the values of the two indicators reach their maximums, which are 2.2032% and 0.7919, respectively. This is because the larger the K_f/K_m, the more prone CO_2 gas is to gas channeling during the injection and shut-in stages. At the same time, the higher the K_f/K_m, the easier CO_2 gas production is, thereby affecting the development effect.

8. Adaptability Analysis of Oil Saturation

Due to the continuous changes in reservoir oil saturation at different developmental stages, the effectiveness of CO_2–oil interactions dynamically varies, resulting in significant development performance differences of reservoirs at different stages [37]. Therefore, in order to study the recovery degree and incremental recovery degree of CO_2 huff and puff under different oil saturations, CO_2 huff and puff simulations were conducted at oil saturations of 0.5, 0.55, 0.6, 0.65, and 0.7 when K_f/K_m was 10. The development effects were compared under different oil saturation levels using incremental recovery and the oil change rate as indicators, and the results are shown in Table 7 and Figure 14.

The development effect curves under different oil saturations are shown above. When K_f/K_m is constant, the increase in the recovery degree and oil change rate increases with the increase in oil saturation. However, the amplitude of changes in the two indicators gradually decreases. When the oil saturation is greater than 0.6, the increase in the recovery degree and oil change rate slows down. When the oil saturation is 0.7, the maximum increases in the recovery rate and oil change rate are 2.0413% and 0.8771, respectively.

Table 7. Development effect under different oil saturation.

Oil Saturation	Increment of Extraction Degree/%	Oil Exchange Ratio
0.5	0.9311	0.4413
0.55	1.2732	0.6236
0.6	2.0024	0.7919
0.65	2.0165	0.8309
0.7	2.0413	0.8771

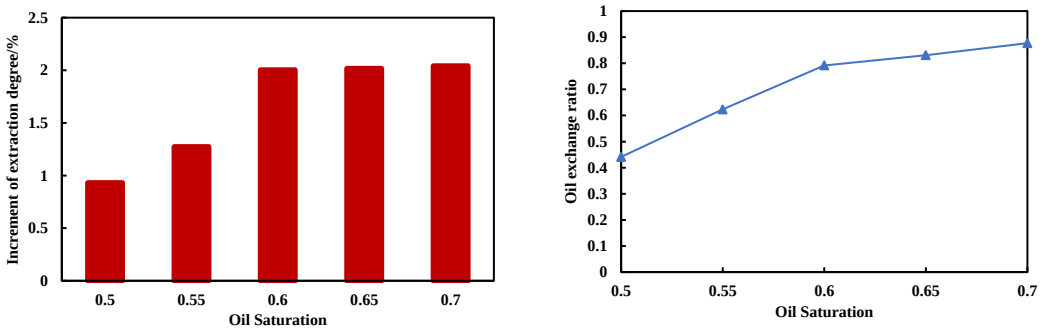


Figure 14. Incremental recovery degree and oil change rate at different S_o: (**a**) increment in extraction degree; and (**b**) oil exchange ratio.

9. K_f/K_m—Oil Saturation Chart Determination

Under different K_f/K_m and oil saturation values, the final increase in the recovery degree and oil change rate exhibit different trends. Therefore, to further explore the development effect of CO_2 huff and puff under the coupling effect of K_f/K_m and oil saturation, a basic model was used to study the K_f/K_m oil saturation adaptability of CO_2 huff and puff and to determine the adaptability limit. Using the incremental recovery degree and oil change rate as reference standards, when the oil saturations are 0.5, 0.55, 0.6, 0.65, and 0.7, K_f/K_m is selected to be 10, 100, and 1000 for CO_2 huff and puff simulation experiments. Then, simulation experiments are conducted to obtain the data points of the recovery degree increment and oil change rate under different schemes. By creating contour maps, the K_f/K_m oil saturation adaptability chart is obtained, as shown in Figure 15.

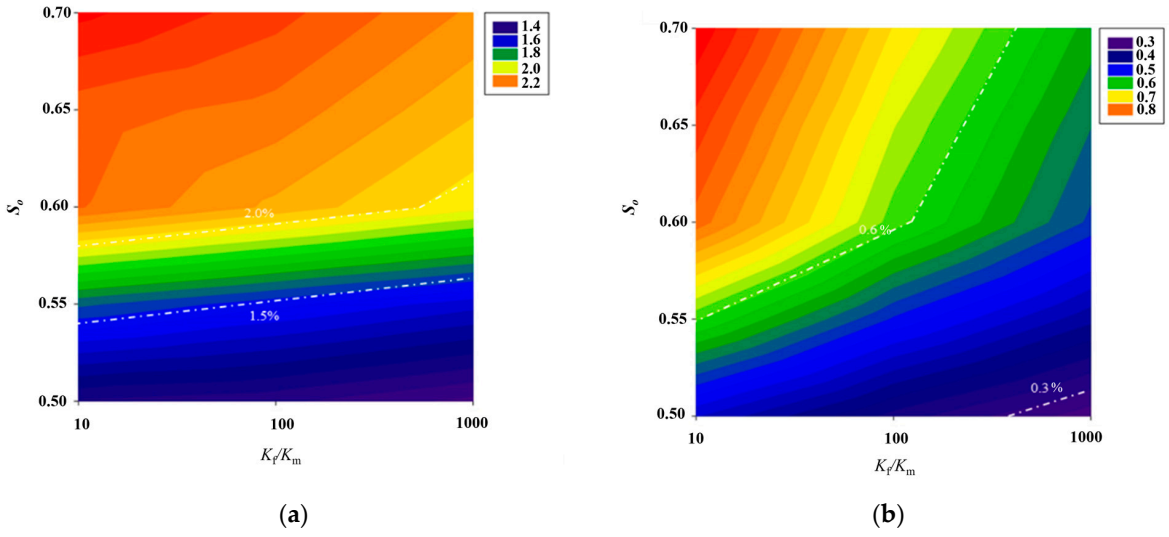


Figure 15. K_f/K_m–S_o chart of CO_2 soaking: (**a**) incremental mining degree chart; and (**b**) oil change rate chart.

It can be seen from the K_f/K_m–S_o chart that with the increase in oil saturation and K_f/K_m, the increase in the recovery degree and oil change rate both increase, and there is no inflection point in the chart. Overall, the better the physical properties of the reservoir and the permeability of the transformed area, the better the development effect of shale oil CO_2 huff and puff. From the perspective of the oil increase effect, when K_f/K_m is 1000 and the increase in CO_2 huff and puff recovery reaches 1.5%, the lower limit of oil saturation is 0.54. When K_f/K_m is 1000 and the increase in the CO_2 recovery rate reaches 2%, the lower limit of oil saturation is 0.57. From the perspective of the oil change effect, when the oil saturation is 0.5 and the CO_2 huff and puff oil change rate reaches 0.3, the lower limit of K_f/K_m is 700.

Finally, when the oil saturation is 0.548 and the CO_2 huff and puff oil change rate reaches 0.6, the lower limit of K_f/K_m is 10. The adaptability limits under different K_f/K_m and oil saturation values can be determined through the CO_2 huff and puff K_f/K_m–S_o chart, which can provide a reference for shale oil CO_2 huff and puff development.

10. Conclusions

A carbon dioxide huff and puff model for shale oil horizontal wells was established based on typical shale oil samples and reservoir physical parameters, and an adaptive evaluation of the development effect of CO_2 huff and puff in horizontal wells was conducted. The following conclusions were obtained:

(1) By correcting the critical parameter of the average pore throat radius and using the fluid p–T phase diagram shift to reflect the nanoconfinement effect, it was found that the corrected p–T phase diagram shifts upwards, causing an increase in bubble point pressure, and thus affecting the properties of each component in crude oil.

(2) By comparing the cases of CO_2 diffusion coefficient consideration and non-consideration, it was found that during the injection and shut-in stages, the CO_2 content and recovery degree in the oil phase of the matrix corresponding to CO_2 diffusion were high.

(3) Taking the incremental recovery rate and oil change rate as references, the development effect of CO_2 huff and puff under the coupling effect of K_f/K_m and oil saturation was explored, and K–S_o charts under different K_f/K_m and oil saturation values were obtained. The chart results show that when K_f/K_m is 1000 and the increases in the CO_2 recovery rate reach 1.5% and 2%, the lower limits of oil saturation are 0.54 and 0.57%, respectively. When the oil saturation is 0.5 and the CO_2 huff and puff oil change rate reaches 0.3, the lower limit of K_f/K_m is 700. Finally, when the oil saturation is 0.548 and the CO_2 huff and puff oil change rate reaches 0.6, the lower limit of K_f/K_m is 10.

Author Contributions: Conceptualization, F.Z.; methodology, F.Z.; validation, M.L.; formal analysis, Y.W.; investigation, S.H.; data curation, Y.W.; writing—original draft preparation, Y.W.; writing—review and editing, M.L. and C.Y.; visualization, C.Y.; supervision, S.H. All authors have read and agreed to the published version of the manuscript.

Funding: This research was funded by the National Natural Science Foundation of China (NO. 52174039) and China Petroleum Strategic Cooperation Technology Special Project (NO. ZLZX2020–02–04).

Data Availability Statement: Data are contained within the article.

Conflicts of Interest: Author Yu Wang was employed by the company Changqing Oilfield Branch No. 1 Oil Production Plant. The remaining authors declare that the research was conducted in the absence of any commercial or financial relationships that could be construed as a potential conflict of interest.

References

1. Zhang, X.; Li, K.; Ma, Q.; Fan, J. Position and prospect of CCUS technology development under carbon neutrality. *China Popul. Resour. Environ.* **2021**, *31*, 29–33.
2. Hu, Y.; Hao, M.; Chen, G.; Sun, R.; Li, S. Technology and practice of CO_2 flooding and storage in China. *Pet. Explor. Dev.* **2019**, *46*, 716–727. [CrossRef]
3. Yang, Y. Research and practice of CO_2 flooding technology for ultra-low permeability reservoirs in Shengli Oilfield. *Pet. Geol. Recovery Effic.* **2020**, *27*, 11–19.
4. Li, D.; Saraji, S.; Jiao, Z.; Zhang, Y. CO_2 injection strategies for enhanced oil recovery and geological sequestration in a tight reservoir: An experimental study. *Fuel* **2021**, *284*, 119013. [CrossRef]
5. Huang, X.; Gu, L.; Li, S.; Du, Y.; Liu, Y. Absolute adsorption of light hydrocarbons on organic–rich shale: An efficient determination method. *Fuel* **2022**, *308*, 121998. [CrossRef]
6. Zeng, T.; Miller, C.S.; Mohanty, K.K. Combination of a chemical blend with CO_2 huff-n-puff for enhanced oil recovery in oil shales. *J. Pet. Sci. Eng.* **2020**, *194*, 107546. [CrossRef]
7. Zhao, P.; Gray, K.E. Finite discrete-element modeling of multifracture propagation in fractured reservoirs. *J. Pet. Sci. Eng.* **2021**, *208*, 109229. [CrossRef]

8. Wang, H. Hydraulic fracture propagation in natural fractured reservoirs complex fracture or fracture networks. *J. Nat. Gas Sci. Eng.* **2019**, *68*, 102911. [CrossRef]
9. Zhang, F.; Dontsov, E. Modeling hydraulic fracture propagation and proppant transport in a two-layer formation with stress drop. *Eng. Fract. Mech.* **2018**, *199*, 705–720. [CrossRef]
10. Deng, B.; Yin, G.; Li, M.; Zhang, D.; Lu, J.; Liu, Y.; Chen, J. Feature of fractures induced by hydrofracturing treatment using water and L-CO_2 as fracturing fluids in laboratory experiments. *Fuel* **2018**, *226*, 35–46. [CrossRef]
11. Jin, L.; Hawthorne, S.; Sorensen, J.; Pekot, L.; Kurz, B.; Smith, S.; Heebink, L.; Bosshart, N.; Torres, J.; Dalkhaa, C.; et al. Extraction of oil from the Bakken shales with supercritical CO_2. In Proceedings of the SPE/AAPG/SEG Unconventional Resources Technology Conference, Austin, TX, USA, 24–26 July 2017.
12. Tovar, F.D.; Barrufet, M.A.; Schechter, D.S. Gas injection for EOR in organic rich shale. part i: Operational philosophy. In Proceedings of the SPE Improved Oil Recovery Conference, Oklahoma City, OK, USA, 14–18 April 2018.
13. Gamadi, T.D.; Elldakli, F.; Sheng, J.J. Compositional simulation evaluation of EOR potential in shale oil reservoirs by cyclic natural gas injection. In Proceedings of the SPE/AAPG/SEG Unconventional Resources Technology Conference, OnePetro, Denver, CO, USA, 25–27 August 2014.
14. Chen, C.; Balhoff, M.; Mohanty, K.K. Effect of reservoir heterogeneity on primary recovery and CO_2 huff-n-puff recovery in shale-oil reservoirs. *SPE Reserv. Eval. Eng.* **2014**, *17*, 404–413. [CrossRef]
15. Orozco, D.; Fragoso, A.; Selvan, K.; Noble, G.; Aguilera, R. Eagle ford huff-n-puff gas-injection pilot: Comparison of reservoir-simulation, material balance, and real performance of the pilot well. *SPE Reserv. Eval. Eng.* **2020**, *23*, 247–260. [CrossRef]
16. Lu, J.; Wang, X.; He, Y.; Yang, C.; Deng, N. Diagenesis and pore evolution of tight sandstone of Chang 7 oil-bearing formation in Fuxian area, Ordos Basin. *J. Northeast Pet. Univ.* **2017**, *41*, 9–20.
17. Li, Z.; Qu, X.; Liu, W.; Lei, Q.; Sun, H.; He, Y. Discussion on reasonable development mode of tight oil in Chang 7 member of Ordos Basin. *Pet. Explor. Dev.* **2015**, *42*, 217–221. [CrossRef]
18. Li, Y.; Shang, Y.; Yang, P. Modeling fracture connectivity in naturally fractured reservoirs: A case study in the Yanchang Formation, Ordos Basin, China. *Fuel* **2018**, *211*, 789–796. [CrossRef]
19. Zhou, X.; Zhang, L.; Fan, K. Current status and progress in research on fracture prediction of low permeability reservoirs in oil and gas basins. *Geol. Rev.* **2006**, *52*, 777–782.
20. Nojabaei, B.; John, R.T.; Chu, L. Effect of capillary pressure on fluid density and phase behavior in tight rocks and shales. In Proceedings of the SPE 159258, SPE Annual Technical Conference and Exhibition, San Antonio, TX, USA, 8–10 October 2012.
21. Barsotti, E.; Tan, S.P.; Saraji, S.; Piri, M.; Chen, J.H. A review on capillary condensation in nanoporous media: Implications for hydrocarbon recovery from tight reservoirs. *Fuel* **2016**, *184*, 344–361. [CrossRef]
22. Pitakbunkate, T.; Balbuena, P.B.; Moridis, G.J.; Blasingame, T.A. Effect of confinement on pressure/volume/temperature properties of hydrocarbons in shale reservoirs. *SPE J.* **2016**, *21*, 621–634. [CrossRef]
23. Li, L.; Su, Y.; Sheng, J.J.; Hao, Y.; Wang, W.; Lv, Y.; Zhao, Q.; Wang, H. Experimental and numerical study on CO_2 sweep volume during CO_2 huff-n-puff enhanced oil recovery process in shale oil reservoirs. *Energy Fuels* **2019**, *33*, 4017–4032. [CrossRef]
24. Lee, J.H.; Lee, K.S. Investigation of asphaltene-derived formation damage and nano-confinement on the performance of CO_2 huff-n-puff in shale oil reservoirs. *J. Pet. Sci. Eng.* **2019**, *182*, 106–304. [CrossRef]
25. Zarragoicoechea, G.J.; Kuz, V.A. Critical shift of a confined fluid in a nanopore. *Fluid Phase Equilibria* **2004**, *220*, 7–9. [CrossRef]
26. Fu, J.; Guo, W.; Li, S.; Liu, X.; Cheng, D.; Zhou, X. Characteristics and exploration potential of multi type Shale oil in Chang 7 Member of Ordos Basin. *Nat. Gas Geosci.* **2021**, *32*, 1749–1761.
27. Zhang, L.; Liu, S.; Yong, R.; Li, B.; Zhao, Y.L. Numerical simulation of staged fracturing horizontal wells in tight reservoirs based on EDFM. *J. Southwest Pet. Univ.* **2019**, *41*, 1–11.
28. Zhu, D.; Hu, Y.; Cui, M.; Chen, Y.; Liang, C.; Cai, W.; He, Y.; Wang, X.; Chen, H.; Li, X. Coupling local grid refinement with embedded discrete fracture model to predict the production capacity of fracturing renovation wells. *Pet. Explor. Dev.* **2020**, *47*, 341–348. [CrossRef]
29. Zhang, D. Research on the method for determining the economic limit production of CO_2 flooding. *China Sci. Technol. Inf.* **2016**, *8*, 122–123.
30. Yuan, Z.; Yang, S.; Zhang, Z.; Wang, M.; Zhang, X. Adaptability evaluation and law simulation of CO_2 injection huff and puff in ultra-low permeability reservoirs. *Unconv. Oil Gas* **2022**, *9*, 85–92.
31. Ding, Z.; Dong, P.; Yang, X.; Ding, D.; Zuo, W.; Pan, H. Numerical simulation of CO_2 miscible flooding in fractured reservoirs considering Molecular diffusion. *Block Oil Gas Field* **2015**, *22*, 245–250.
32. Jiang, J.; Liu, Q.; Wang, J. Calculation method of effective action radius of carbon dioxide huff and puff in tight reservoir. *Sci. Technol. Eng.* **2020**, *20*, 2216–2222.
33. Luo, Y.; Sun, L.; Wu, Z.; Zhao, X.; Xiao, H. A CO_2 huff and puff productivity prediction model for horizontal wells in tight reservoirs based on diffusion coefficient changes. *Sci. Technol. Eng.* **2021**, *21*, 3588–3594.
34. Li, D.; Hou, J.; Zhao, F.; Wang, S.; Yue, X. Study on molecular diffusion coefficient and solubility of carbon dioxide in crude oil. *Oilfield Chem.* **2009**, *26*, 405–408.
35. Du, F.; Nojabaei, B. Estimating diffusion coefficients of shale oil, gas, and condensate with nano-confinement effect. *J. Pet. Sci. Eng.* **2020**, *193*, 107–362. [CrossRef]

36. Han, W. Study on CO_2 Huff and Puff Effect of Fractured Horizontal Wells in Tight Oil Reservoir. Master's Thesis, China University of Petroleum, Beijing, China, 2018.
37. Yang, X. Optimization of Numerical Simulation Parameters of Shale Oil CO_2 Huff and Puff. Master's Thesis, China University of Petroleum, Beijing, China, 2021.

Disclaimer/Publisher's Note: The statements, opinions and data contained in all publications are solely those of the individual author(s) and contributor(s) and not of MDPI and/or the editor(s). MDPI and/or the editor(s) disclaim responsibility for any injury to people or property resulting from any ideas, methods, instructions or products referred to in the content.